

Co-doped Y_2O_3 optical functional nanoparticles and novel self-assembly squama-like aggregates

X.G. Liu^{*}, J. Du, D.Y. Geng, S. Ma, J.M. Liang, M. Tong, Z.D. Zhang

Shenyang National Laboratory for Material Science, Institute of Metal Research and International Centre for Material Physics,
Chinese Academy of Sciences, 72 Wenhua Road, Shenyang 110016, PR China

Received 23 January 2007; received in revised form 8 March 2007; accepted 8 March 2007

Available online 12 March 2007

Abstract

Co-doped Y_2O_3 optical functional nanoparticles with size of 4–10 nm have been synthesized by the plasma arc-discharge method. Meanwhile, novel three-dimensional squama-like macro-aggregates were self-assembled by disordered nanoparticles synthesized simultaneously in the arc-discharge process. The formation mechanism of the aggregates is ascribed to the periodic coagulation of Y nanoparticles. The valence states of Co in Y_2O_3 lattice can be determined as +2 from XPS spectrum with an etching depth of 6 nm. For Co-doped Y_2O_3 nanoparticles, upon excitation with 426 nm, a red emission (620 nm) has been observed which originates from ${}^4A_2({}^4F) \rightarrow {}^4T_1({}^4P)$ d–d transitions of Co^{2+} ions in tetrahedral co-ordination.

© 2007 Elsevier B.V. All rights reserved.

Keywords: Nanostructures; X-ray diffraction; Luminescence; Magnetic measurements

1. Introduction

Yttria has received great attentions in various fields of advanced functional materials, due to its excellent properties such as a high dielectric constant, a low absorption in a broad range (from near-UV to IR), a superior electrical break-down (>3 MV/cm) and a low leakage current onto silicon substrates [1]. Yttria is one of the best hosts for lanthanide ions, because its ionic radius and crystal structure are very similar to those of many lanthanide oxides [2]. Doping with a variety of lanthanide ions can yield materials with different fluorescent spectra, such as Eu for red, Tb for green, Dy for yellow and Tm for blue [3]. Regarding optical materials doped by transition-metal ions, only a little work has so far been reported. Co^{2+} is a kind of laser active ion. Tetrahedrally coordinated Co^{2+} in many bulk crystals, such as $Co:Y_3Al_5O_{12}$ and $Co:MgAl_2O_4$, can exhibit intense absorption at 1.54 μm , and these materials can be used as the Q-switched material [4]. Sun et al. reported that Co^{2+} -doped $Y_3Al_5O_{12}$ nanocrystallites exhibit a red emission (630 nm) upon excitation with 420 nm [4]. Lakshminarayana et al. found that

in Co^{2+} -doped B_2O_3 –ZnO–PbO glasses, upon excitation with 580 nm, a red emission (625 nm) has been observed which originates from $E^2({}^2G) \rightarrow {}^4A_2({}^4F)$ transition of Co^{2+} ions in tetrahedral co-ordination [5]. However, little work has been reported about the emission spectrum of Y_2O_3 nanoparticles doped by Co^{2+} ions until now.

Nanoparticles can be prepared by various methods with different mechanisms, including physical, chemical, physico-chemical and mechanical ones. The structural, physical and biomedical properties of nanoparticles depend sensitively on the sample-preparation processes [6]. A wide variety of synthesis techniques have been developed for the production of pure and doped nanopowders, including wet chemical methods [7], laser ablation [8], sol–gel [4] and combustion [9]. Different sets of parameters for each synthesis method determine the structural and optical properties of the final products. As a well-known method for producing the nanoparticles, the arc-discharge method has been widely used for the formation of fullerenes and related materials [6]. For instance, the iron group metals (Fe, Co, Ni) were encapsulated within hollow graphitic cage [10]. To the best of our knowledge, there has been no report on the studies of optical functional nanoparticles prepared by arc-discharge method.

^{*} Corresponding author.

E-mail address: liuxg@imr.ac.cn (X.G. Liu).

During preparation of the nanoproducts, the nanounits, such as nanoparticles, nanoclusters, nanowires and nanorods, can be also self-assembled into the novel structural aggregates by several routes, including the chemical vapor deposition [11], the laser vaporization–condensation [12], the charge transferring [13], the electron irradiation deposition [14], the organic reagent-assisted method [15], the solution–liquid–solid method [16] and the catalytic vapor–liquid–solid growth [17]. With these routes, various nanoscale or microscale aggregates can demonstrate novel architectures, including web-like, spherical, nanowire-like, network, tree-like and fishbone-like aggregates. In a recent work, we successfully prepared the novel coral-like aggregates self-assembled by GdAl_2 nanocapsules by the arc-discharge process, which showed the feasibility of the arc-discharge technique [18].

In this paper, we synthesized Co-doped Y_2O_3 nanoparticles by the arc-discharge method and investigated the optical properties. At the same time, regularly aligned three-dimensional macro-aggregates self-assembled by the nanoparticles were simultaneously synthesized in the arc-discharge process.

2. Experimental procedures

The Co-doped Y_2O_3 nanoparticles, which self-assembled into the squama-like aggregates, were synthesized by the arc-discharge method with modified strategies. In purified argon atmosphere, an $\text{Y}_{67}\text{Co}_{33}$ (at%) alloy button was prepared by arc-melting Y and Co flakes of 99.9 wt% purity at least four times so that the components were homogeneous. The experimental procedure of the arc-discharge was similar to that in the previous reports [18,19], but with some changes on the arc-discharge furnace. Fig. 1 represents the schematic diagram of the arc-discharge furnace with a segmental baffle in front of the target. The cathode was a tungsten needle with a diameter of 3 mm. The anode target (i.e., the $\text{Y}_{67}\text{Co}_{33}$ alloy button) was placed into one pit of a water-cooled copper crucible. The distance and the angle between the anode and the cathode were about 3 mm and 60° , respectively. A mixture gas of Ar (20000 Pa) and H_2 (4000 Pa) was introduced into an evacuated chamber (6.6×10^{-3} Pa), before a potential was applied between the cathode and the anode. During the arc-discharging process, the current was maintained at 100 A for 5 h, while the voltage was maintained at 16 V. After being passivated in argon atmosphere (0.02 MPa) for 24 h, squama-like macro-aggregates (Fig. 2) in a large-area were collected from the surface of the segmental baffle in front of the target.

X-ray powder diffraction (XRD) pattern was recorded with a D/max-2000 diffractometer at a voltage of 50 kV and a current of 250 mA with Cu $\text{K}\alpha$ ($\lambda = 1.54056 \text{ \AA}$). The architecture of the aggregates self-assembled by nanoparticles was characterized by a Philips SSX-550 scanning electron microscope (SEM), with an emission voltage of 20 kV. The detailed morphology of the

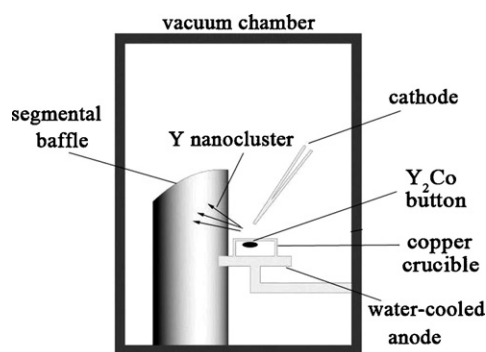


Fig. 1. Schematic diagram of the arc-discharge furnace employed to synthesize the nanoparticles.

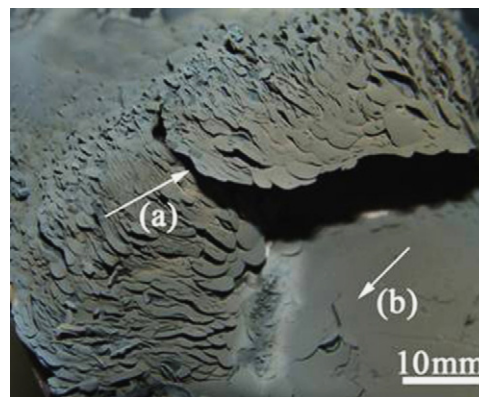


Fig. 2. Macro-morphology of the aggregates on the segmental baffle. The arrows (a) and (b) mark squama-like and film-like architectures, respectively.

nanoparticles was observed by a transmission electron microscope (TEM JEOL-2010) with an emission voltage of 200 kV. The emission spectrum of the nanoparticles was measured using an FL4500 fluorescence spectrophotometer. X-ray photoelectron spectroscopy (XPS) measurements were performed on ESCALAB-250 with a monochromatic X-ray source (an aluminum $\text{K}\alpha$ line of 1486.6 eV energy and 150 W) to characterize the valence of Co in the Y_2O_3 at a depth of 6 nm. The magnetic properties of the nanoparticles were measured on a Quantum Design MPMS-7 superconducting quantum interference device (SQUID).

3. Results and discussion

The macro-morphology of the aggregates, deposited on the segmental baffle during the arc-discharge, is shown in Fig. 2. It is clearly seen that there are the squama-like architectures (marked by the arrow (a)) and the film-like structures (marked by the arrow (b)) with thickness of 2 mm. The macro-morphology of the aggregates deposited on the segmental baffle is greatly different from that of the aggregates deposited on the anode (copper crucible) [18,19]. Unfortunately, the aggregates with the squama-like architectures are too soft to be observed in details by SEM. Nevertheless, the morphology of the film-like structures was examined by SEM, as shown in Fig. 3, which might provide with information on the initial stage of the growth of the squama-like architectures. The SEM image indicates that the film-like structures with some isolated particles are not dense, which distinctly differ from the previous reports [18,19]. The

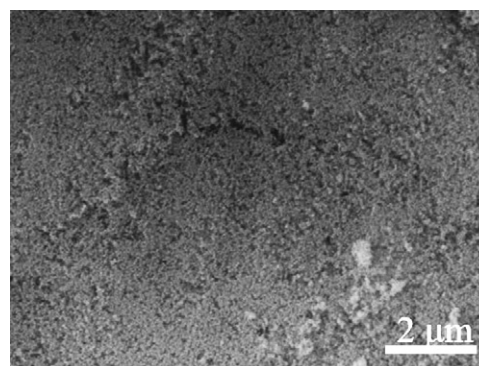


Fig. 3. SEM image of the aggregates with film-like structures marked by the arrow (b) in Fig. 2.

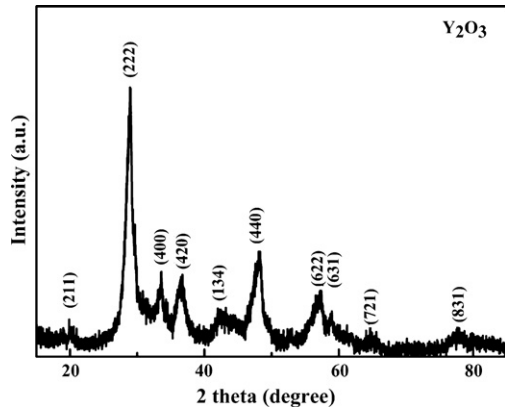


Fig. 4. X-ray diffraction (XRD) spectrum of the Co-doped Y_2O_3 nanoparticles constructing aggregates.

significant difference in the micro-morphology can be related to the formation and coagulation behavior of the nanoparticles [20].

The formation mechanism of nanoparticles in plasma is that matter clusters with a high activity exist in the plasma, which could exchange rapidly the energy with the reacted matter clusters, beneficial to the reaction between them. When the reacted matter clusters leave the high temperature flam tail region of the

plasma, the rapid decrease of the temperature lets the clusters be in the over saturation state in dynamic equilibrium; thus they are dissociated. The rapid cooling leads to the nucleation of crystallites and the formation of nanoparticles. At the same time, nanoparticles with high speed are diffused around the region of the plasma. Most of the Y nanoparticles approach the surface of the segmental baffle with a certain angle incidence, due to the low density of Y (Fig. 1). Meanwhile, the coarse surface of the segmental baffle also provides more chances to the nanoparticles at initial times of the growth to capture incident particles and form the nucleation of the aggregates [19]. The source materials for the growth of the aggregates can be directly supplied by the process of oblique angle incident. At the initial stage of the growth of the squama-like architectures, Y nanoparticles are rapidly coagulated to form film-like structure, due to the low temperature of segmental baffle. Film-like structures elevate the surface temperature of segmental baffle. Afterwards, Y nanoparticles are slowly coagulated in a certain period, which induces the formation of the squama-like aggregates. Yttrium nanoparticles, due to higher surface energy, are completely oxidized to form Y_2O_3 nanoparticles when they are exposed to air.

The XRD pattern in Fig. 4 shows the phase components of the as-prepared products prepared by arc-discharging $Y_{67}Co_{33}$

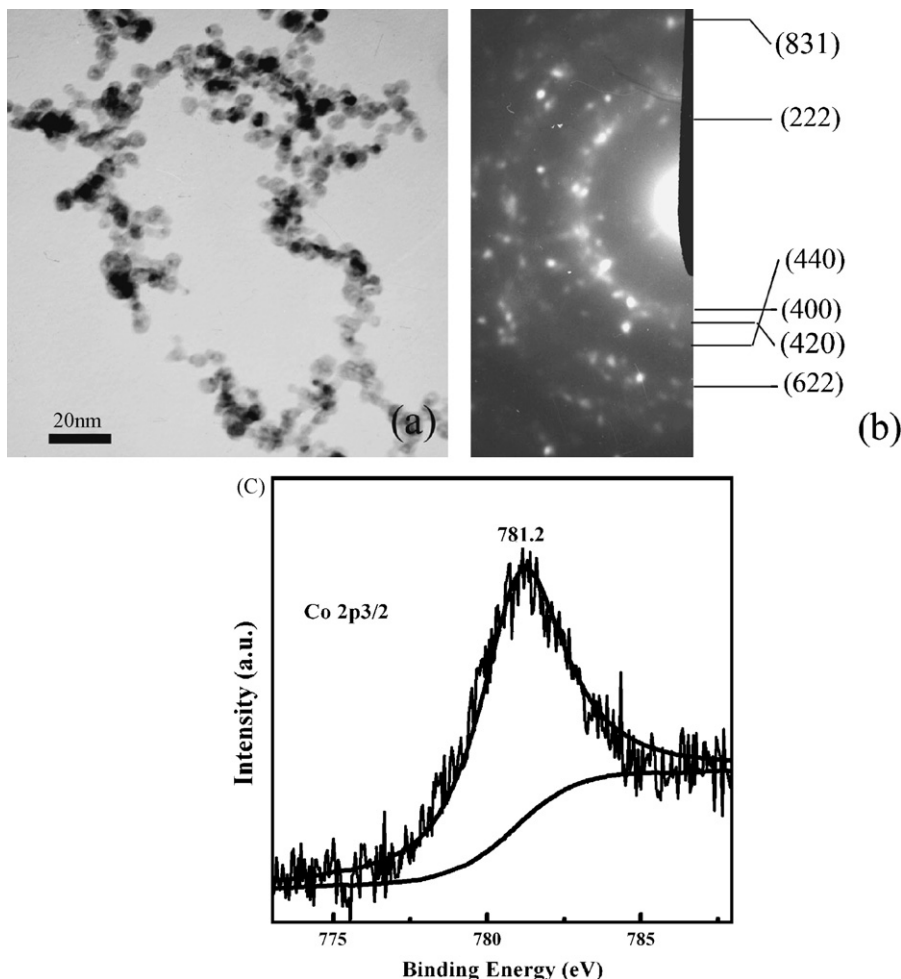


Fig. 5. (a) TEM morphology of the Co-doped Y_2O_3 nanoparticles. (b) The corresponding electron diffraction patterns of (a). (c) XPS spectrum and corresponding fitting curve of the Co in Y_2O_3 at a depth of 6 nm.

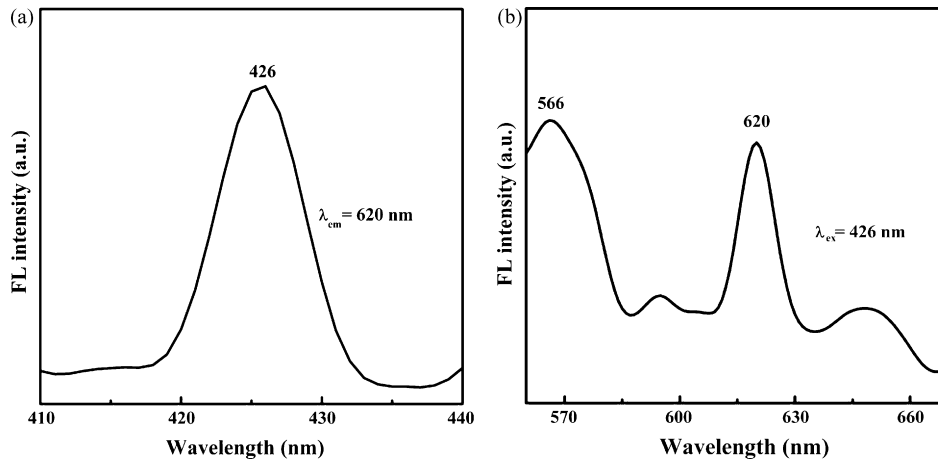


Fig. 6. Excitation (a) and emission (b) spectra of Co-doped Y_2O_3 nanoparticles.

alloy. All XRD peaks could be indexed to the single-phase body-centered cubic Y_2O_3 . The result is different from the previous reports that fcc (or hcp) cobalt exists in nanoparticles prepared by arc-discharging cobalt-based alloy [19,21–23]. According to the (6 2 2) diffraction peak, the calculated lattice parameter of the as-prepared Y_2O_3 nanoparticles is 10.65 Å, which is bigger than 10.59 Å of the pure Y_2O_3 phase. Y_2O_3 is the structure of c-RE (rare earths) style, the six tetrahedral gaps are occupied by O ions and the other tetrahedral gaps without O ions [24]. And ionic radius of O^{2-} (0.132 nm) is bigger than that of Co^{2+} (0.072 nm). The lattice expansion suggests that some cobalt ions may enter into the remanent tetrahedral gaps without oxygen ions in the body-centered cubic Y_2O_3 lattice. In addition, the size of the particles is estimated to be 4–6 nm, according to the half-width of XRD peaks of Y_2O_3 .

Fig. 5(a) shows TEM morphologies of the Y_2O_3 nanoparticles. The Y_2O_3 nanoparticles are of irregular spherical shape, and the diameter distribution is from 4 to 10 nm, as measured from Fig. 5(a), which is well consistent with the sizes estimated above. Besides the irregular shapes, the nanoparticles show also coarse surfaces. The irregular shapes and the coarse surfaces of the nanoparticles are ascribed to the rapid quenching and the coexistence of different phases during the arc-discharge process [25]. A common feature of the samples is that they have some agglomerates. Compared with the previous report [26], the Y_2O_3 nanoparticles show higher dispersivity in Fig. 5(a). Different synthetic conditions caused some differences in the dispersivity of nanoparticles [26]. From the selected area electron diffraction (SAED) pattern (Fig. 5(b)), the formation of Y_2O_3 can be determined from the characteristic diffraction rings, indicating the characteristic lattice planes (2 2 2), (4 0 0), (4 2 0), (4 4 0), (6 2 2) and (8 3 1) of Y_2O_3 , which is consistent with the XRD results. The valence states of Co in Y_2O_3 lattice can be determined as +2 from the binding energy peak of 781.2 eV [27], which is shown in the XPS spectrum with an etching energy depth of 6 nm (Fig. 5(c)). The existence of Co^{2+} in Y_2O_3 can be explained that a small amount of dissociated Co evaporate into bcc phase as doped ions in the arc-discharging [21].

The emission spectrum at room temperature of Co-doped Y_2O_3 nanoparticles in visible region is shown in Fig. 6(b), and

the excited wavelength is 426 nm in Fig. 6(a). The intense emission bands appeared at the wavelengths of 566 and 620 nm, respectively. The position of the emission peak of Co-doped Y_2O_3 nanoparticles is similar to that of $Y_3Al_5O_{12}$ nanocrystals doped with tetrahedral Co^{2+} ions in the visible region [4]. This indicates that Co^{2+} ions locate in the tetrahedral sites of Y_2O_3 nanoparticles. In its neutral charge state, the Co^{2+} ions have an [Ar] $3d^7$ electron configuration. The atomic 4F ground state splits under the influence of the tetrahedral component of the crystal field into a 4A_2 ground state and $^4T_2 + ^4T_1$ excited states. The smaller trigonal distortion and spin–orbit interaction split the ground 4A_2 state into $E_{1/2} + E_{3/2}$ [28]. The emission peaks around 620 and 566 nm in the visible range are derived from separately $^4A_2(^4F) \rightarrow ^4T_1(^4P)$ and $^4A_2(^4F) \rightarrow ^4A_1(^4G)$ transitions of tetrahedral Co^{2+} ions [29,30]. Because the dopant ions affect the band gap structure of the host materials [31], the emission spectra of the Co-doped Y_2O_3 present a red shift, compared with that reported early in Ref. [27]. Measurements at room temperature generally exhibit some inhomogeneous broadening of the spectral lines. In addition, small particles are more susceptible to surface defects and disorder than larger particles. Disordered states contribute to the broadening of the spectrum [2].

Magnetization measurement shows a distinct ferromagnetic behavior. Fig. 7 represents magnetic hysteresis loop at 300 K of the Co-doped Y_2O_3 nanoparticles. The curve in Fig. 7 shows

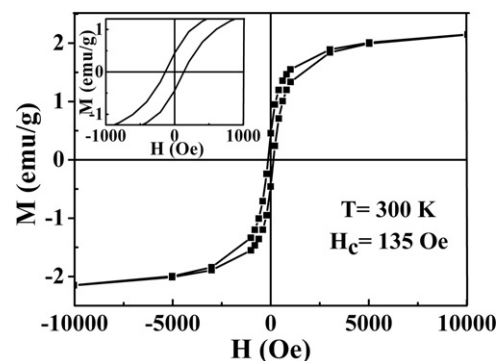


Fig. 7. Magnetic hysteresis loop at 300 K of Co-doped Y_2O_3 nanoparticles. The inset shows magnified portion of the curves.

obvious hysteresis with the coercive field H_c of 135 Oe at 300 K, which is higher than that of Co-doped ZnO films, but the saturation magnetization M_s is smaller than that of Co^{2+} in a tetrahedral crystal field ($3.0 \mu_B/\text{Co}$) [32]. It is reasonable to assume that the observed optical and magnetic properties are intrinsic nature of Co element in Y_2O_3 nanoparticles.

4. Conclusion

In conclusion, Co-doped Y_2O_3 nanoparticles have been synthesized using the arc-discharge method. At the same time, novel three-dimensional squama-like macro-aggregates were self-assembled by Y_2O_3 nanoparticles synthesized simultaneously in the arc-discharge process. The nanoparticles' size is in the range of 4–10 nm. The valence states of Co in Y_2O_3 lattice can be determined as +2 from XPS spectrum with an etching energy depth of 6 nm. For Co-doped Y_2O_3 nanoparticles, upon excitation with 426 nm, a red emission (620 nm) has been observed which originates from ${}^4\text{A}_2({}^4\text{F}) \rightarrow {}^4\text{T}_1({}^4\text{P})$ d–d transitions of Co^{2+} ions in tetrahedral co-ordination. The arc-discharge method opens up a new way of synthesizing optical functional materials.

Acknowledgment

This work was supported by the National Natural Science Foundation of China under grant number 50331030.

References

- [1] Y.C. Wu, S. Parola, O. Marty, J. Mugnier, *Opt. Mater.* 27 (2004) 21–27.
- [2] D. Dosev, B. Guo, I.M. Kennedy, *J. Aerosol Sci.* 37 (2006) 402.
- [3] F. Vetrone, J.C. Boyer, J.A. Capobianco, A. Speghini, M. Bettinelli, *Nanotechnology* 15 (2004) 75.
- [4] Z.H. Sun, D.R. Yuan, X.L. Duan, X.C. Wei, H.Q. Sun, C.N. Luan, Z.M. Wang, X.Z. Shi, D. Xu, M. Lv, *J. Cryst. Growth* 260 (2004) 171.
- [5] G. Lakshminarayana, S. Buddhudu, *Spect. Acta: Part A.* 63 (2006) 295.
- [6] Z.D. Zhang, in: H.S. Nalwa (Ed.), *Encyclopedia of Nanoscience and Nanotechnology*, vol. 6, American Scientific, California, 2004, pp. 77–160.
- [7] R. Bazzi, M.A. Flores-Gonzalez, C. Louis, K. Lebbou, C. Dujardin, A. Brenier, W. Zhang, O. Tillement, E. Bernstein, P. Perriat, *J. Lumin.* 102–103 (2003) 445.
- [8] H. Eilvers, B.M. Tissue, *Chem. Phys. Lett.* 251 (1996) 74.
- [9] J. Hao, S.A. Studenikin, M. Cocivera, *J. Lumin.* 93 (2001) 313.
- [10] Z.D. Zhang, *J. Mater. Sci. Technol.* 23 (2007) 1.
- [11] K.A. Dick, K. Deppert, M.W. Larsson, T. Martensson, W. Seifert, L.R. Wallenberg, L. Samuelson, *Nat. Mater.* 3 (2004) 380.
- [12] M.S. Elshall, S.T. Li, D. Graiver, U. Pernisz, *ACS Symposium Series*, vol. 622, 1996, pp. 79–99.
- [13] K. Naka, H. Roh, Y. Chujo, *Langmuir* 19 (2003) 5496.
- [14] S.O. Cho, E.J. Lee, H.M. Lee, J.G. Kim, Y.J. Kim, *Adv. Mater.* 18 (2006) 60.
- [15] Q.Y. Lu, F. Gao, D.Y. Zhao, *Nanotechnology* 13 (2002) 741.
- [16] A.K. Boal, F. Ilhan, J.E. Derouchev, T. Thurn-Albrecht, T.P. Russell, V.M. Rotello, *Nature* 404 (2000) 6779.
- [17] Y.Q. Zhu, W.K. Hsu, W.Z. Zhou, M. Terrones, H.W. Kroto, D.R.M. Walton, *Chem. Phys. Lett.* 347 (2001) 337.
- [18] S. Ma, D.Y. Geng, W.S. Zhang, W. Liu, X.L. Ma, Z.D. Zhang, *Nanotechnology* 17 (2006) 5406.
- [19] X.G. Liu, D.Y. Geng, S. Ma, J.M. Liang, Z.D. Zhang, *Nanotechnology*, in preparation.
- [20] Y.J. Leng, S.H. Chan, K.A. Khor, S.P. Jiang, P. Cheang, *J. Power Sources* 117 (2003) 26–34.
- [21] S. Ma, Y.B. Wang, D.Y. Geng, J. Li, Z.D. Zhang, *J. Appl. Phys.* 98 (2005) 094304.
- [22] D.Y. Geng, Z.D. Zhang, W.S. Zhang, P.Z. Si, X.G. Zhao, W. Liu, K.Y. Hu, Z.X. Jin, X.P. Song, *Scripta Mater.* 48 (2003) 593.
- [23] P.Z. Si, R.S. Turtelli, R. Grossinger, A. Reissner, M. Kuepferling, Z.D. Zhang, *J. Alloys Compd.* 379 (2004) 82–86.
- [24] Z.T. Zhang, J.Y. Zhang, *Inorganic Photoluminescence Materials and their Application*, Chemical Industry Press, Beijing, 2005, pp. 19–21.
- [25] P.Z. Si, E. Brück, Z.D. Zhang, I. Skorvanek, J. Kovac, M. Zhang, *Mater. Res. Bull.* 39 (2004) 1005.
- [26] L. Wen, X.D. Sun, Q. Lu, G.X. Xu, X.Z. Hu, *Opt. Mater.* 29 (2006) 239.
- [27] B.J. Tan, K.J. Klabunde, P.M.A. Sherwood, *J. Am. Chem. Soc.* 113 (1991) 855.
- [28] C. Liu, F. Yun, H. Morkoc, *J. Mater. Sci.* 16 (2005) 555.
- [29] S. Ramachandran, A. Tiwari, J. Narayan, *Appl. Phys. Lett.* 84 (2004) 5255.
- [30] K.J. Kim, Y.R. Park, *Appl. Phys. Lett.* 81 (2002) 1420.
- [31] P. Yang, M.K. Lu, C.F. Song, D. Xu, D.R. Yuan, *Phys. Stat. Sol. (b)* 231 (2002) 106.
- [32] X.C. Liu, E.W. Shi, Z.Z. Chen, H.W. Zhang, L.X. Song, H. Wang, S.D. Yao, *J. Cryst. Growth* 296 (2006) 135.